A Parametric $G1$-continuous Rounded Wing Tip Treatment for Preliminary Aircraft Design

Marshall C. Galbraith* and Robert Haimes†
Department of Aeronautics & Astronautics, MIT, Cambridge MA

Flat wing tips can cause convergence difficulties for Euler and Reynolds Averaged Navier-Stokes analysis of preliminary aircraft design configurations. However, for preliminary design, the details of the wing tip may not be the primary focus of the study, these convergence problems can be remedied by rounding the wing tips. This paper presents a method for generating rounded wing tips that are governed by a single design parameter and are $G1$-continuously connected to the wing. While a single parameter is not sufficient for a detailed wing tip design, it enables a smaller design space for preliminary design. Both sharp and blunt trailing edge airfoils are considered. The rounded wing tip formulation is implemented as part of the Engineering Sketch Pad software framework and the lofting routines are analytically differentiated via operator overloaded automatic differentiation to provide parametric sensitivities for gradient based design optimization.

Nomenclature

r	=	tip ratio parameter
$\vec{x}_0$	=	general semi-ellipse centroid
$\vec{a}, \vec{b}$	=	general semi-ellipse conjugate diameters
$\vec{x}_U, \vec{x}_L$	=	sampled points from upper and lower lofted surfaces
$\vec{b}_U, \vec{b}_L$	=	unit tangent vectors from upper and lower lofted surfaces
u, v	=	surface parametric coordinates
t	=	curve parametric coordinates
$\vec{C}(t)$	=	parametric Cartesian curve
$\vec{S}(u,v)$	=	parametric Cartesian surface
Symbols		
$\|\cdot\|$	=	magnitude of 3-dimensional Cartesian components
$\vec{\cdot}$	=	Cartesian 3-dimensional components

I. Introduction

The Computational Aircraft Prototype Synthesis (CAPS) [1, 2] project seeks to create a highly integrated design environment with a dynamic process that enables analysis of configurations with tools spanning a spectrum of disciplines and fidelities at any stage of design maturity. Rather than relying on a single geometric representation of a vehicle, the CAPS system uses a parametric geometric model which can generate multiple geometric representations of the same vehicle using a single set of design parameters. Thus, the appropriate geometric representation is always available for a desired analysis regardless of the analysis fidelity and discipline.

For the CAPS project, the core parametric geometric model is generated using Engineering Sketch Pad (`ESP`). `ESP` is a feature-based parametric solid modeler where the geometry is generated by executing a user defined build recipe via the Open-source Constructive Solid Modeler (`OpenCSM`) [3, 4] scripting language. The build scripts can be generated by hand or interactively via the `ESP` GUI. The build recipe can use standard primitive solids, solids grown from sketches, applied features, Boolean operators, and transformations. In addition, either compiled or scripted user defined primitives/functions are supported. Furthermore, `ESP` allows for attribution directly on the geometry providing a natural means of specifying information such as boundary conditions, grid spacings, and mass and stiffness properties for shell structural modeling. The general framework of `ESP` allows the construction of a range of parametric geometric configurations and hence provides the flexibility to perform optimization on a large variety of conventional

and unconventional aircraft planforms. Some example configurations generated with ESP are shown in Fig. 1. In addition, fast analytic sensitivities of the BRep geometry definition w.r.t. design parameters are available for most primitives and operations.

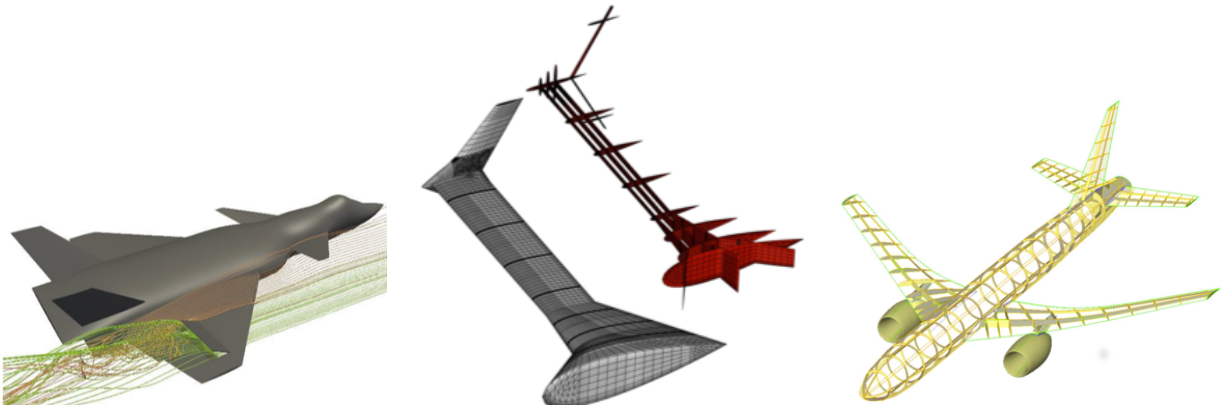

Fig. 1 Example geometries generated with ESP.

Parametric geometric models typically consist of multiple components, e.g. wing, fuselage, tail, engines. An example of such a parametric model is shown in Fig. 2. Using this core model, suitable "views" of the geometry are constructed for a given analysis tool using the OpenCSM language. Thus, a single set of design parameters can be used to construct geometric definitions suitable for Vortex-Lattice methods, Full-Potential, or Euler/Reynolds Average Navier-Stokes (RANS) Computational Fluid Dynamics (CFD) analysis as shown in Fig. 3.

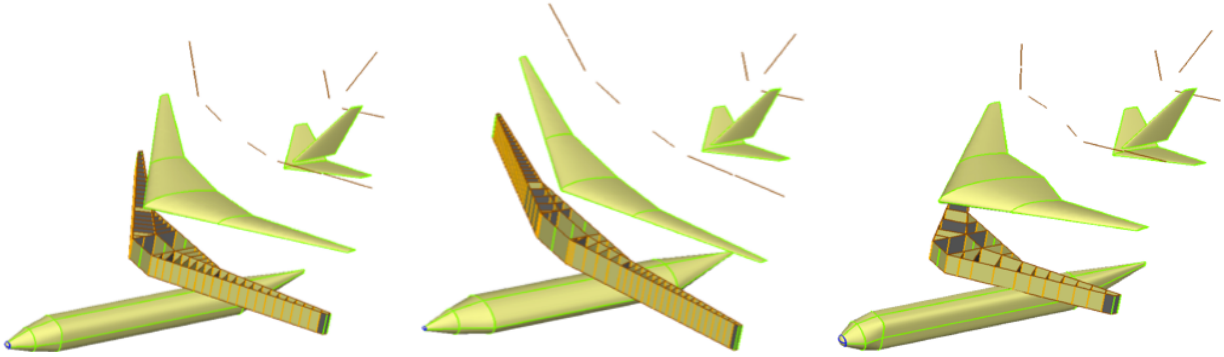

Fig. 2 Parametric variations of conceptual components embodied in a transport design model.

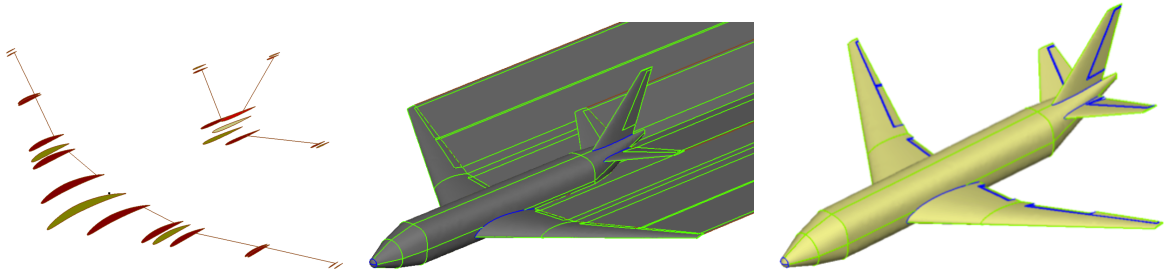

(a) Vortex Lattice (b) Full-Potential (c) Euler/RANS

Fig. 3 Views of an aircraft design model for three levels of aerodynamic analysis.

Analysis robustness is critical for a design optimization cycle. While the lower fidelity linearized CFD analysis such

as vortex lattice methods will always produce a result, the discrete non-linear Euler/RANS equations can be difficult to solve. In particular, strong gradients around flat wing tips can lead to non-physical solutions with near zero (or negative) pressures/temperature. While this can sometimes be resolved by adjusting the grid distribution in the vicinity of the flat wing tip, this is not a automatable solution for a design optimization cycle.

A simpler solution to mitigate CFD solver convergence issues associated with flat wing tips is to round the tip. This is only one reason why grid generation software such as `WINGCAP` in Chimera Grid Tools[5] and the Boeing unpublished `TIPCAP`* can generate rounded grids when the geometric wing tip is flat. However, generating rounded wing tips using mesh generation software is challenging for unstructured grids and it effectively excludes the rounded tip design parameters from the design optimization process. Hence, software tailored specifically to generate parametric air vehicle geometry, such as Vehicle Sketch Pad (OpenVSP)[6], Rapid Aircraft Geometry Engine (RAGE)[7], Boeing proprietary General Geometry Generator (GGG)[8], GENAIR[9], and GeoMACH[10] to name a few, include the options to generate rounded wing tips.

While the option to generate rounded wing tips is common for air vehicle geometry software, the specific algorithms used to produce the rounded wing tips is hardly discussed in the literature. Usually papers are understandably dedicated to the larger suite of capabilities and the generation of rounded wing tips is considered one feature among many others. For example, Ref. [7] states that that RAGE can generate elliptic wing tips as part of lofting airfoil sections, but does not provide further details. Similarly, Ref. [10] simply states that any rounded wing tips are $C1$-continuous. An algorithm for generating rounded wing tips similar, but not identical, to the one presented here appears to be implemented in OpenVSP†, though the authors have not found any published literature related to it.

This paper present the detailed algorithm for generating rounded wing tips as part of the `ESP` geometry generation software. The rounded tip formulation is built upon the general *lofting* algorithm in `ESP` [11], which already includes a special degeneracy treatment for generating fuselages with up to $C2$-continuity from nose to tail and is $G1$-continuous circumferentially. By design, the rounded tip is also $G1$-continuous to ensure the rounded tip aligns with any taper, sweep, or twist associated with the lofted airfoil sections. A single design parameter gives control over the elongation of the tip.

The remaining of this paper is organized as follows: the BRep terminology used here is first outlined and followed by the $G1$-continuous general elliptic formulation in Section II. The topological and lofting treatment for blunt trailing edge wings is discussed in Section III. The verification of analytic parametric sensitivity calculation for lofted wings with rounded tips is presented in Section IV.

A. BRep Terminology

Boundary Representations (BReps) are the standard data model that holds both the geometric and topological entities that support the concept of a *solid*, as well as other non-manifold aggregations. For the sake of clarity all BRep topological entities will be capitalized in this paper. That is, a Node is the topological entity that refers to a point, where an Edge has an underlying curve and is usually bounded by two Nodes, and etc. See Ref. [12] for a complete description of this BRep terminology. Note that surfaces are parameterized with u and v coordinates, e.g. $\vec{S}(u, v)$, and curves are parmeterized by a t coordinate, e.g. $\vec{C}(t)$. Surface and curve tangent vectors can be computed by differentiation the surface or curve w.r.t. the parametric coordinate. This will be utilized in the rounded tip formulation.

BRep's topological entities are required to "close" the model because the Nodes that bound an Edge are probably not on the underlying curve. Also, Edges that bound a Face (through the Loops) do not necessarily sit on the supporting surface. However, for a valid closed *solid* all that is required is that the bounding objects (Nodes/Edges) be within a specified tolerance of the higher dimensioned entity (Edges/Faces). Therefore, for any precision higher than the tolerance, gaps and overlaps may exist in the geometry definition. BRep tolerances are generally much larger than values associated with double precision floating-point arithmetic, hence the issue.

II. $G1$-continuous General Elliptic Tip Formulation

The rounded tip implementation is built upon the *lofting* algorithm (called *blend* in `ESP`) presented in Ref. [11]. An example of a wing, with aspect ratio of two, lofted using the *blend* algorithm using three sharp trailing edge NACA0024 airfoil sections is shown in Fig. 4. The lofting produces B-spline geometric surfaces by connecting BRep Edges that occur in the same order when traversing the Loop of Edges in each lofted section. Because each airfoil section is

*Personal communication with Dr. John C. Vassberg, The Boeing Company

†By execution of the software and inspection of the open source code.

constructed in ESP with upper and lower Edges, the loft algorithm generates upper and lower B-spline surfaces from each of the set of Edges. The lofted B-spline surfaces achieve $G1$-continuity around the leading edge by matching the tangent vectors at the end Nodes of the section curves. The underlying uv-parametrization of the lofted B-splines surfaces has, by construction, the u parameter running circumferentially and v running in the lofted direction. The geometry is closed (made a *solid*) by using the starting and ending sections as caps during the topological assembly of the loft. In this example, the mid section is repeated three times to produce a $C0$ break in the surfaces.

The tip rounding formulation is design around the following principals:

- Minimal topological modifications relative to planar caps
- Produces circular cross sections (with the parameter set to 1.0)
- Minimal number of parameters
- Preserves $G1$-continuity with the upper and lower surfaces

To minimize the topological changes, the rounded tip seeks to only replace the underlying cap Face on the tip of the wing. This means that when the airfoils have sharp trailing edges, the rounded tips do not introduce any topological change (additional Edges or Faces) relative to the capped topology. For sharp trailing edges, the rounded tip algorithm assumes that each section is only comprised of two edges and hence the loft only produces a single upper and single lower B-spline surface. This assumption is consistent with all airfoil generators available in ESP. The algorithm only assumes that the sections are constructed with two Edges, there is no assumption that the sections are airfoil shapes.

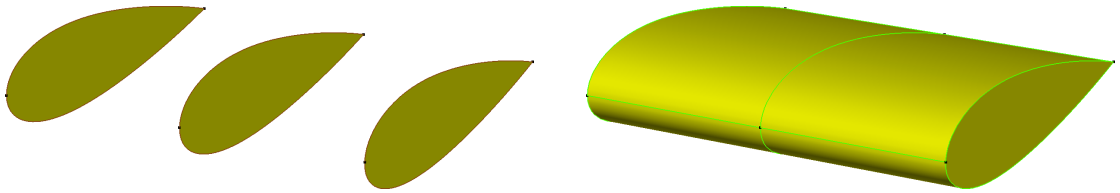

(a) NACA0024 airfoil sections

(b) Lofted wing

Fig. 4 Lofted wing constructed from airfoil sections

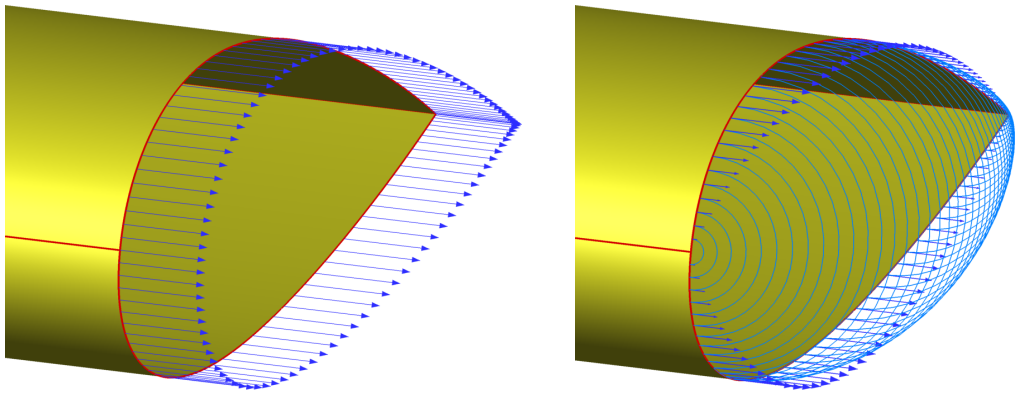

(a) Surface sampling and unit tangent vectors

(b) $\vec{C}(t)$ tangent vectors and circular curves

(c) Top view of scaled tangent vectors and circular curves

Fig. 5 Components for rounded B-spline construction

Rather than using the original planar section, the rounded tip algorithm constructs a new rounded B-spline surfaces to cap off the geometry. The rounded tip surface is constructed by first sampling coordinates, $\vec{x}_U$ and $\vec{x}_L$, and normalized tangent vectors, $\vec{b}_U$ and $\vec{b}_L$, (computed from the surface v-derivative) at the end of the upper and lower lofted surfaces. The samples are taken from the surface u-knot locations (as well as three point in-between knots) as shown in Fig. 5a. By design, when a rounded tip is desired, the upper and lower surfaces are lofted with compatible knot sequences such that the sampling always results in pairs of points. A set of analytic curves are then constructed using these sampling points as illustrated in 5b.

The analytic curves are governed by the parametric equation for a general semi-ellipse in 3-dimensional space

$$\vec{C}(t) = \vec{x}_0 + \vec{a}\cos(\pi t) + \vec{b}\sin(\pi t) \qquad t \in [0, 1] \tag{1}$$

where x_0 is the centroid and $\vec{a}$ and $\vec{b}$ are the conjugate diameters (which in general are not perpendicular). In the circumstance where $\vec{a} \perp \vec{b}$ and $\|\vec{a}\| = \left\|\vec{b}\right\|$ the general semi-ellipse reduces to a semi-circle. The centroid and diameter $\vec{a}$ are computed from the sampled coordinates as

$$\vec{x}_0 = \frac{1}{2}(\vec{x}_U + \vec{x}_L) \tag{2}$$

$$\vec{a} = \frac{1}{2}(\vec{x}_U - \vec{x}_L), \tag{3}$$

which is required so that the endpoints of the curves match up with the upper and lower surfaces. More choices are available for the second diameter $\vec{b}$. Here, the authors have first chosen to introduce the single user defined parameter r to define the magnitude of $\vec{b}$ as

$$\left\|\vec{b}\right\| \equiv r\,\|\vec{a}\| \quad r \geq 0. \tag{4}$$

Thus, setting $r = 1$ gives circular curves, and $r \neq 1$ results in elliptical curves. In addition, $r = 0$ produces a linear interpolation between $\vec{x}_U$ and $\vec{x}_L$ and hence recovers the original planar capped tip. One possible choice for the direction of $\vec{b}$ is simply the unit average of $\vec{b}_U$ and $\vec{b}_L$, i.e.

$$\vec{b} \equiv \vec{b}_0 = r\,\|\vec{a}\|\,\frac{\frac{1}{2}\left(\vec{b}_U + \vec{b}_L\right)}{\left\|\frac{1}{2}\left(\vec{b}_U + \vec{b}_L\right)\right\|}. \tag{5}$$

This choice ensures that the curve is always elliptic, however, the curve would only be $G1$-continuous with the upper and lower surfaces when $\vec{b}_U = \vec{b}_L$. Another choice that guarantees $G1$-continuity between the curve and upper/lower surfaces is to linearly interpolate the direction vector between $\vec{b}_U$ and $\vec{b}_L$, i.e.

$$\vec{b} \equiv \vec{b}_{G1}(t) = r\,\|\vec{a}\|\,\frac{\left(\vec{b}_U(1-t) + t\,\vec{b}_L\right)}{\left\|\frac{1}{2}\left(\vec{b}_U + \vec{b}_L\right)\right\|}. \tag{6}$$

Note that $\vec{b}_{G1}(\frac{1}{2}) \equiv \vec{b}_0$ in general, and $\vec{b}_{G1}(t) \equiv b_0$ when $\vec{b}_U = \vec{b}_L$.

Examples of the general semi-elliptical ($\vec{b} = \vec{b}_0$) curves and the $G1$-continuous general semi-elliptical ($\vec{b} = \vec{b}_{G1}(t)$) curves are shown in Fig. 6. Figure 6a illustrates that when $\vec{b}_U = \vec{b}_L$ the $G1$-continuous semi-ellipse is identical to the general semi-ellipse. However, when the tangent vectors are diverging (Fig. 6a) or converging (Fig. 6c) the $G1$-continuous general semi-elliptical curves matches the tangent vectors while the general semi-ellipses do not.

The same lofting algorithm used create the upper/lower surfaces is used to construct a B-spline surface with the set of analytic curves. The curves are are sampled at 23 uniformly spaced t-parameter points, and the u-knot sequence running along the curves of the lofted surface is also equally spaced. The resultant B-spline surface has a degeneracy at the leading and trailing edges, and the tangent vectors at the end point of the curves are used to impose the B-spline end conditions circumferentially. The magnitude of the tangent vectors do not require any scaling as the circumferential u-parametric coordinate of the B-spline matches the t-parametric coordinate of the analytic curves. Thus, if the curves are $G1$-continuous with the upper and lower surfaces, then the rounded tip B-spline surface will be $G1$-continuous with the lofted surfaces.

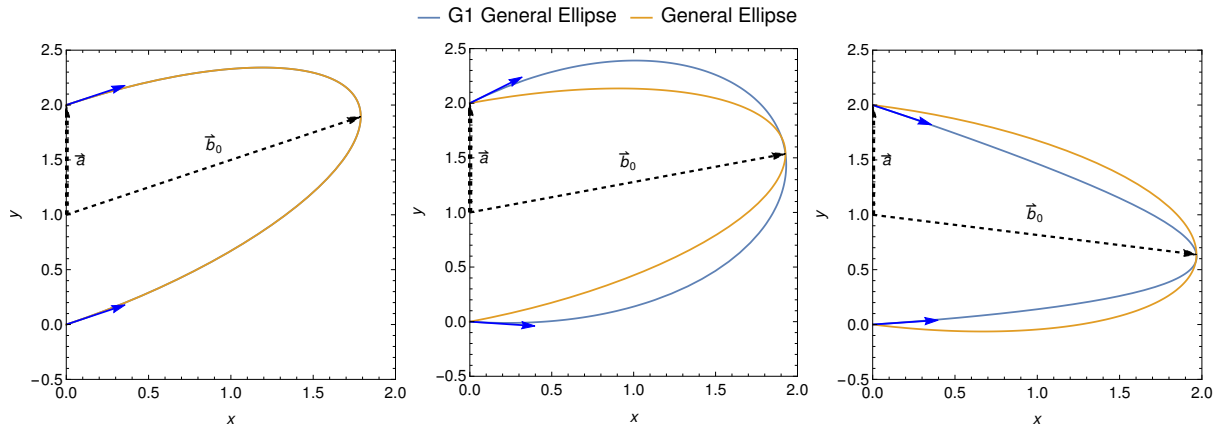

(a) Parallel tangent vectors (b) Diverging tangent vectors (c) Converging tangent vectors

Fig. 6 $G1$-continuous general ellipse and general ellipse curves, $r = 2$

Figure 7 shows the lofted wing from Fig. 4 with $G1$-continuous general semi-ellipse rounded tips where the right tip has $r = 1$ and the left tip with $r = 4$. In this case, the right rounded tip has a circular cross section while the left tip is elliptic. To illustrate the $G1$-continuity of the rounded tips, the mid airfoil section of the lofted wing shown Fig. 8 is thickened to a NACA0050 airfoil. While the right tip remains close to circular, the left wing tip is thinned significantly. However, both sides $G1$-continuity between the rounded tip and the lofted surfaces. Similarly, $G1$-continuity is preserved when the tip airfoil sections are thickened to NACA0050 as shown in Fig. 9. Furthermore, when the wing is swept as shown in Fig. 10, the rounded tip naturally follows the sweep of the wing.

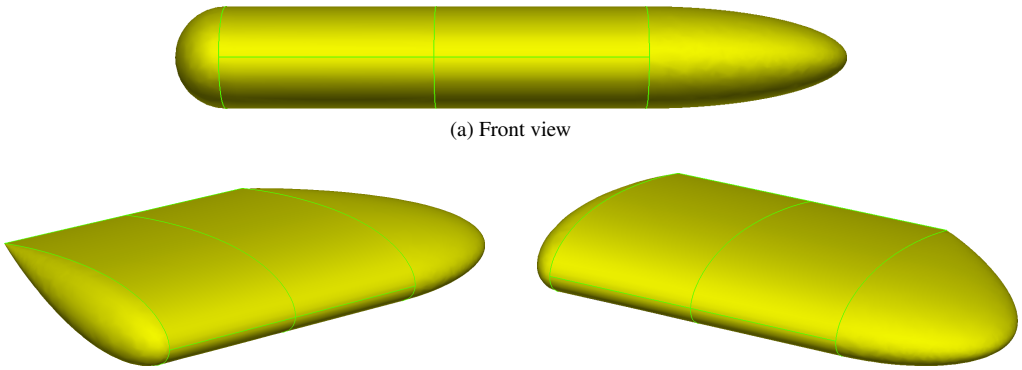

(a) Front view

(b) Right tip $r = 1$ (c) Left tip $r = 4$

Fig. 7 Lofted wing from NACA0024 sections with $r = 1$ and $r = 4$ rounded tips

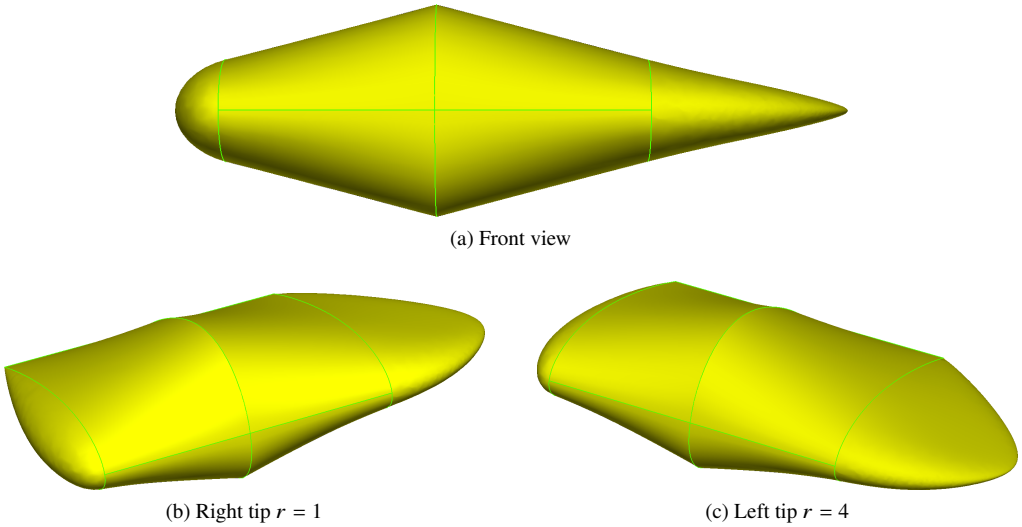

(a) Front view

(b) Right tip $r = 1$

(c) Left tip $r = 4$

Fig. 8 Lofted wing from NACA0050 mid and NACA0024 tip sections with $r = 1$ and $r = 4$ rounded tips

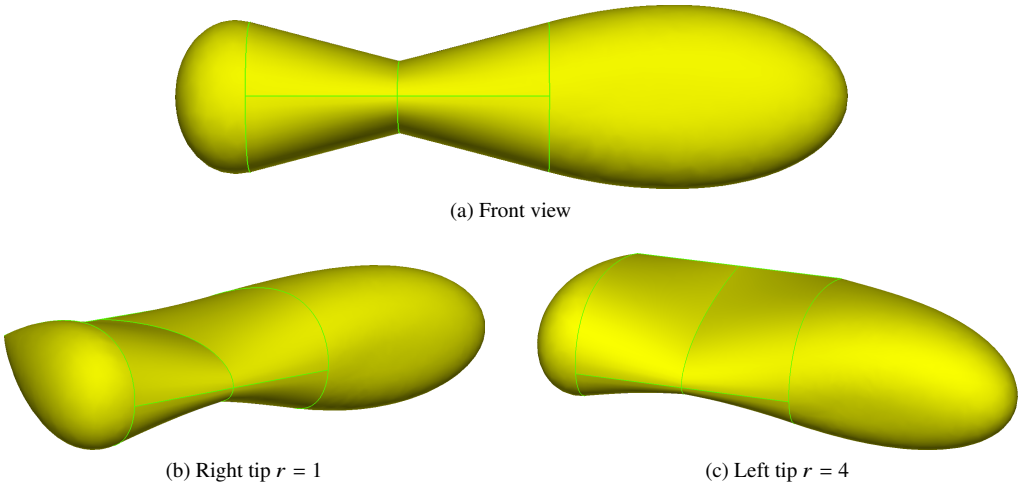

(a) Front view

(b) Right tip $r = 1$

(c) Left tip $r = 4$

Fig. 9 Lofted wing from NACA0024 mid and NACA0050 tip sections with $r = 1$ and $r = 4$ rounded tips

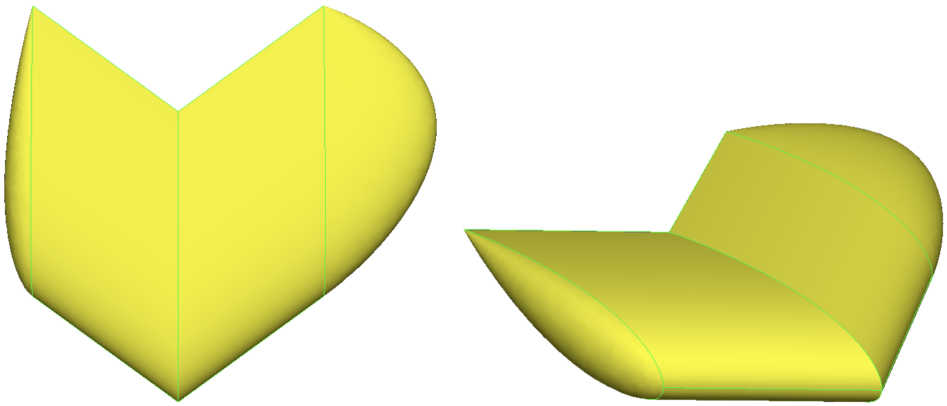

(a) Top view

(b) Iso-view

Fig. 10 Lofted wing with 20° sweep with $r = 1$ and $r = 4$ rounded tips

The tangent vectors $\vec{b}_U$ and $\vec{b}_L$ in the examples shown thus far have been co-planar. However, $G1$-continuous general ellipse curves also work when the tangent vectors are not co-planar; this is demonstrated by rotating the mid airfoil section by 90° to introduce twist in the lofted surface as shown in Fig. 11. Since $\vec{b}_U$ and $\vec{b}_L$ are no longer co-planar, the $G1$-continuous general semi-elliptical curves are also not planar. The complete twisted wing is shown in Fig. 12. The smooth transition from the wing to the rounded tips near the leading and trailing edges of the wing is notable.

While this relatively simple formulation is capable of generating a wide range of rounded wing tip shapes, it is possible to produce poor or self-intersecting shapes. As shown in Fig.13, under some circumstances where the tangent vectors from the surfaces are convergent and the parameter r is too large, the $G1$-continuous general semi-elliptical curve can produce a cusped or worse, a self-intersecting curve. However, in the author's experience, these degeneracies are rarely encountered, and can always be remedied by reducing the value of r. For example, the lofted wing in Fig. 14 has a mid section airfoil of NACA0075. The right tip is rounded with $r = 1$ and produces a valid rounded tip. However, a value of $r = 4$ applied to the left tip produces the self-intersecting curves. Note though that the self-intersection may not occur if tangent vectors are not co-planar. For example, the propeller bade shown in Fig. 15 without any twist has a self intersecting rounded tip. However, introducing the twist as shown in Fig. 16 produces a valid geometry.

Another possible degeneracy occurs when different curves are intersecting. This is possible if the tangent vectors on from the lofted upper and lower surfaces are converging and the value of r is large. An example of this is shown in Fig.17, where the wing is lofted from a NACA0024 mid section and NACA0099 tip sections with a taper ratio of 0.1 and a leading edge sweep of 30°. The left tip with $r = 4$ is intersecting due to the curves from near the trailing edge crossing with the curves from the leading edge. However, reducing the parameter to $r = 1$ produces a valid shape for the right wing tip.

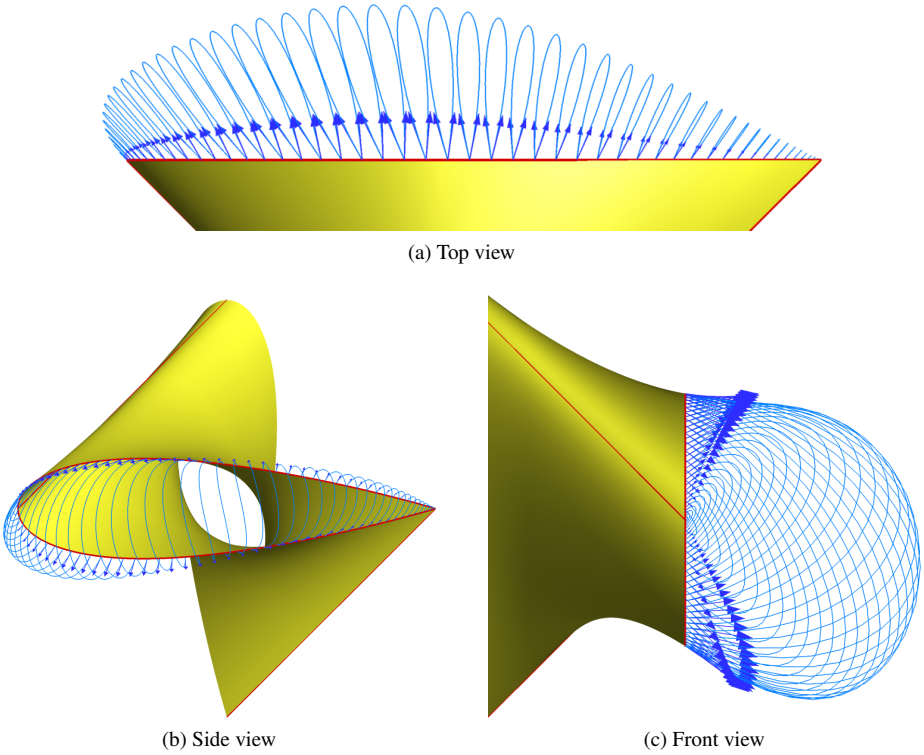

(a) Top view

(b) Side view

(c) Front view

Fig. 11 Left tip curves for twisted lofted wing, $r = 2$

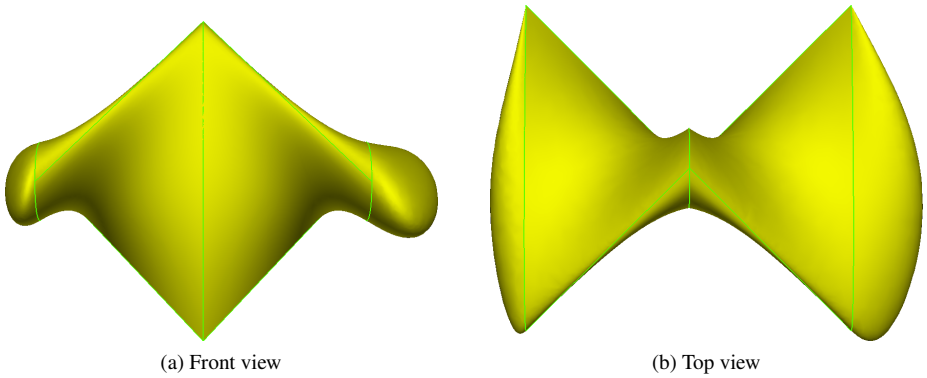

(a) Front view (b) Top view

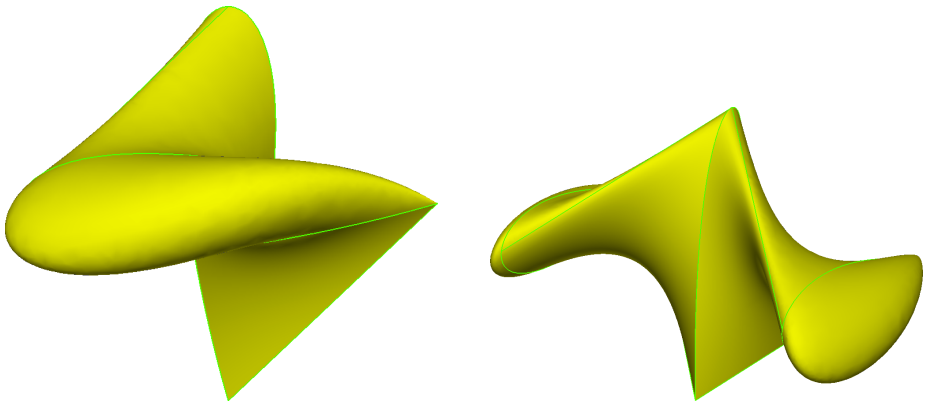

(c) Side view (d) Iso view

Fig. 12 Lofted wing with mid section rotated 90° and right $r = 1$ and left $r = 2$ rounded tips

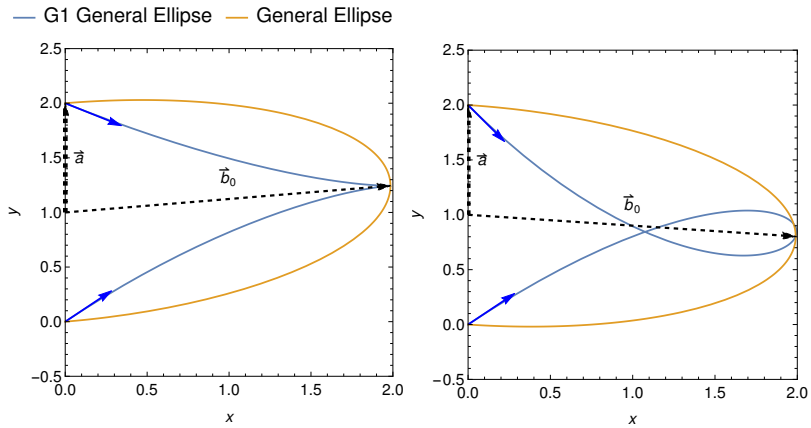

(a) Cusped curve (b) Self intersecting curve

Fig. 13 Degenerate $G1$-continuous general ellipse, $r = 2$

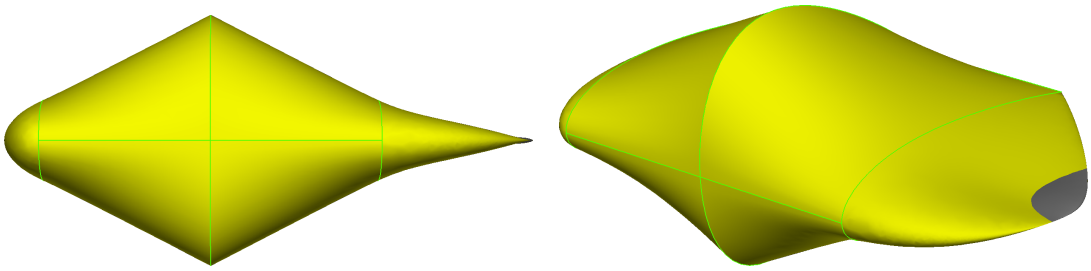

(a) Front view (b) Left tip $r = 4$

Fig. 14 Lofted wing from NACA0075 mid and NACA0024 tip section with self intersecting tip

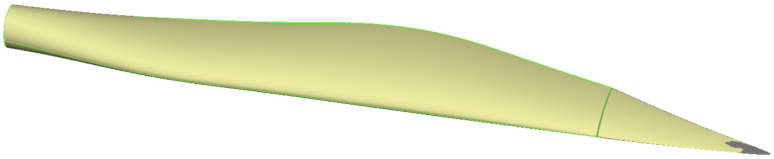

Fig. 15 Propeller blade without twist with $r = 40$ self-intersecting rounded tip

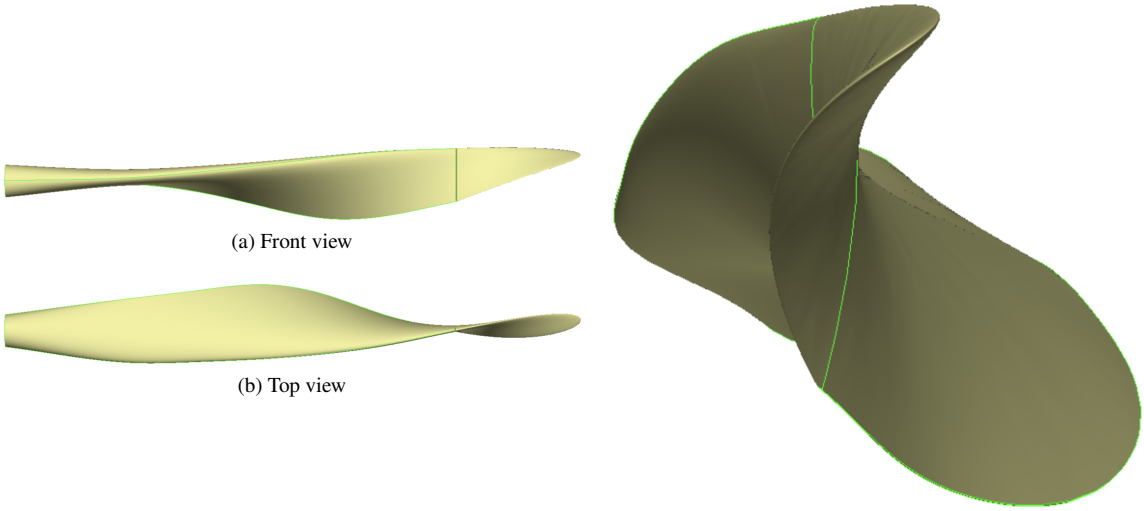

(a) Front view

(b) Top view

(c) View of tip twist

Fig. 16 Propeller blade with $r = 40$ rounded tip

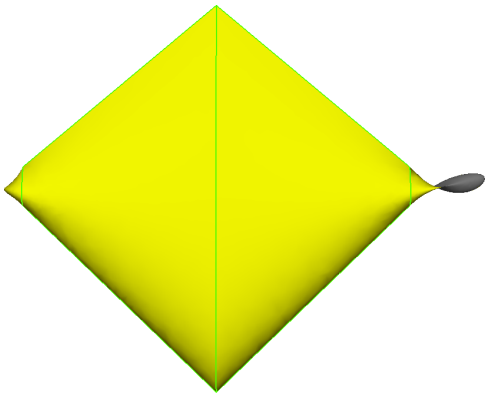

(a) Top view

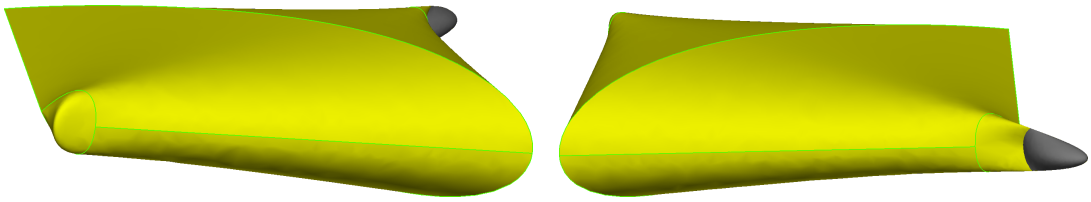

(b) Right tip $r = 1$ (c) Left tip $r = 4$

Fig. 17 Self-intersecting tip due to converging leading/trailing edge tangent vectors

III. Blunt Trailing Edges

Airfoil sections in ESP with blunt trailing edges are represented with three Edges as shown in Fig. 18a; upper, lower, and a straight trailing Edge. When lofted, these airfoil sections produce a wing with upper, lower, and trailing edge surfaces shown in Fig. 18b. With a sharp trailing edge, the last curved used to loft the rounded tip surface is a single point as shown in Fig. 19a. However, with a blunt trailing edge the last curve is open, as shown in Fig. 19b, and the area under this curve needs to be closed in order to form a *solid* shape. One possibility would be to generate a single B-spline surface for this curve independent of the lofted trailing edge surface. However, this would require this separate surface to be represented by a Face separate from the lofted surface. As such, a rounded wing tip with $r > 0$ would be topologically different from a rounded tip with $r = 0$ where the curve has is reduced to a vertical line.

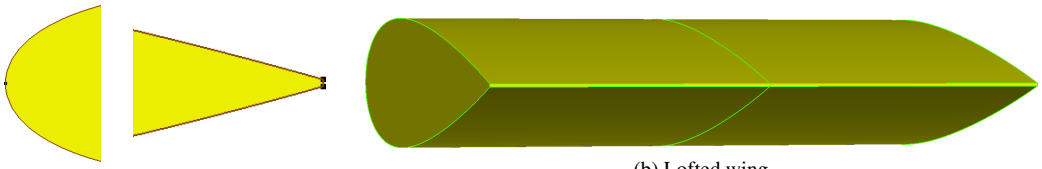

(a) Leading and trailing edge of blunt NACA0024 airfoil

(b) Lofted wing

Fig. 18 Lofted wing with blunt trailing edge

Instead of creating a separate surface, the authors have chosen to include the open curve as part of the lofting to produce the trailing edge surface. To do this, the the blunt trailing edge surface parameterization is modified to include the rounded curve. The surfaces colored by the u-parameter of a blunt lofted wing are shown in Fig. 20a. Here, the u-parameterization travels from the lower Edge to the upper Edge of the blunt trailing edge surface, and the v-parameterization ends at the vertical edge associated with the airfoil section. An extension of this parameterization to the curve is shown in Fig. 20b. Here, the curve is split into two topological Edges associated with $u = 0$ and $u = 1$ iso-lines of the surface. The end of the v-parameterization now ends in a degenerate Node rather than a vertical Edge. This modification is comparable to "pinching" the vertical Edge in 20a down to a zero length without collapsing the

trailing edge surface.

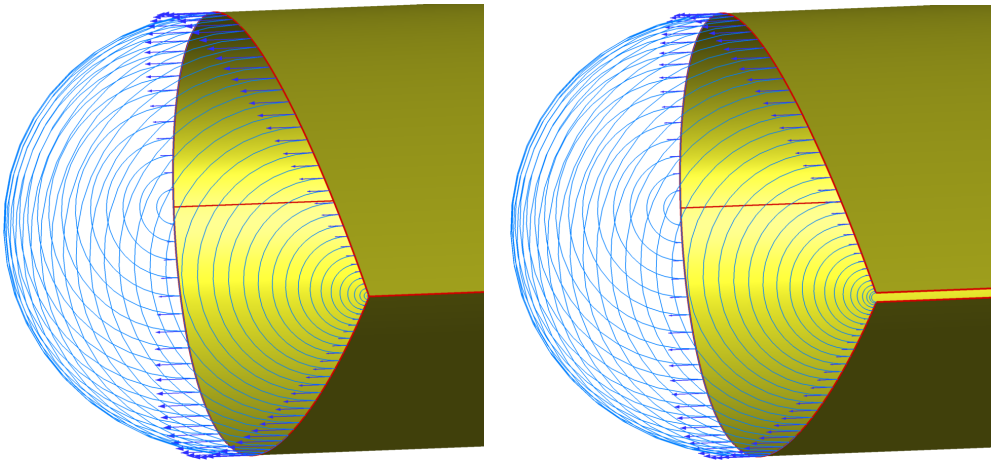

(a) Sharp trailing edge (b) Blunt trailing edge

Fig. 19 Open curve with blunt trailing edge

By splitting the tip curve into two edges at $t = 0.5$, the curve can now be included in the lofting construction of the trailing edge surface. However, in order to make sure the geometry is closed, the analytic curve at the trailing edge is not sampled but instead the corresponding spline curve is extracted from the rounded spline surface and used for the trailing edge surface construction. To extend the trailing edge surface loft into the tip curve, the spline curve is sampled at the u-knots of the rounded tip surface along the upper and lower halves of the curve. Importantly, because the rounded tip surface is constructed with a uniform u-knot sequence, the v-knot spacing of the trailing edge surface can be matched to the u-knot sequence of the rounded tip surface. In addition to sampling the curve, the tangent vectors of the curve at $t = 0.5$ are used to impose slope end conditions in the u-direction at $u = 0$ and $u = 1$ of the surface. This ensures that the lofted trailing edge surface matches with the rounded tip surface. Finally, because the curve extends along the tangent lines of the upper and lower surfaces of the lofted wing, the v-knots are duplicated at the airfoil section to produce a $C1$ line in the surface.

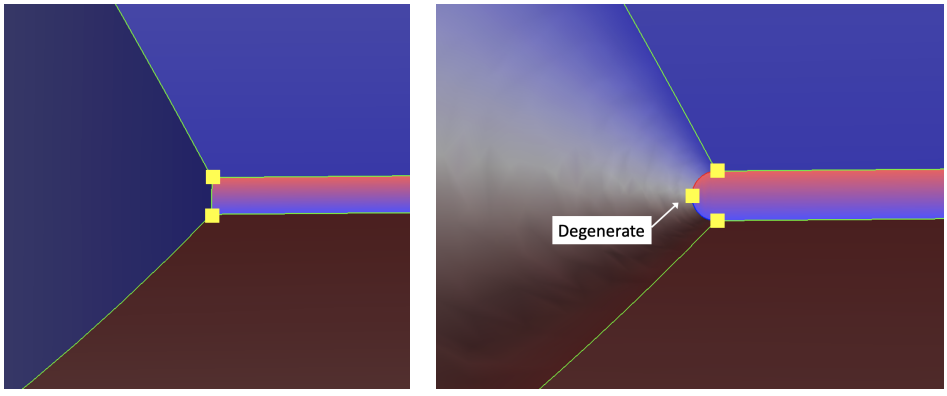

(a) Blunt tip (b) Rounded tip

Fig. 20 Blunt trailing edge topology with surfaces colored by surface u-parameter (blue $u = 0$, red $u = 1$)

IV. Parametric Sensitivities

Both the 1- and 2-dimensional spline fitting routines in `EGADS` are differentiated via operator overloaded automatic differentiation[13]. The knot sequence for spline fits are typically computed from an approximation of arc-length. This can cause causes significant difficulties in computing parametric sensitivities as the knot sequences is also functionally (and non-linearly) dependent on the parameter. However, the use of automatic differentiation readily accounts for this non-linearity. The differentiated spline fitting routines enable computation of sensitivities of fitted curves and surfaces to design parameters.

An example parameterized half wing is shown in Fig. 21. The wing is lofted from three NACA airfoil sections. All three airfoils are parameterized by the same *thickness*, *camber*, and *maxloc* parameters (*maxloc* is the location where the maximum camber occurs). The position and chord of the tip airfoil section is set by the *span*, *sweep*, and *taper* parameters, where as the position and chord for the mid airfoil section is set by the average *span* and *taper*, but is independent of *sweep*. While this is not a typical parameterization of a wing, it produces some additional curvature in the wing that increases the non-linearity of the surface dependence on the design parameters. Finally, the *rtip* parameter represents r for the rounded tip.

Parametric sensitivities computed via finite differencing[14] are used to verify the analytic sensitivity calculation. This is accomplished by first assuming that the analytic sensitivities represent the true value, and and computing the error in the finite difference sensitivity relative to the analytic sensitivity for decreasing step sizes. If the analytic sensitivity is correct, the error in the finite difference should converge at a rate consistent with the order of the finite differencing scheme. As a 1^{st}-order finite difference scheme is used here, the error should also decay at a rate of one.

The L^{∞}-norm of the inner product between the sensitivity and surface normal with decreasing step size for both blunt and sharp trailing edge versions of the wing are shown in Fig. 22. The sensitivity error is evaluated on a discrete tessellation of all Faces, Edges, and Nodes. For both wings, the error in the finite difference sensitivities of all parameters decay at the expected 1^{st}-order rate. The error in sensitivity w.r.t. *rtip* is machine zero at the largest step size for the wing with a sharp trailing edge, and increases with decreasing pertubation size. This is expected as the rounded tip is linearly dependent on the *rtip* parameter when the trailing edges is sharp. This is not seen for the blunt trailing edge as the the blunt trailing edges surfaces is non-linearly dependent on the rounded tip surface.

Lofted Wing Parameters		
sharpte	0	NACA airfoil sharp TE switch
thickness	0.16	NACA airfoil thickness
camber	0.12	NACA airfoil camber
maxloc	0.4	NACA airfoil max location
span	1.0	Span of the wing
taper	0.5	Ration of tip/root chord
sweep	20.	Sweep of tip airfoil (deg)
rtip	4.0	Ratio for rounded tip

(a) Airfoil sections

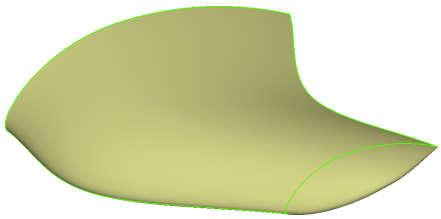

(b) Lofted Wing Top view

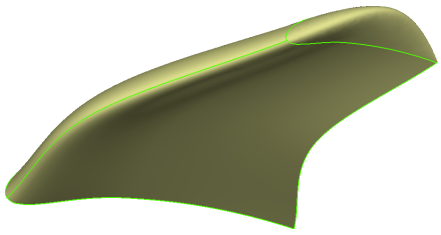

(c) Lofted Bottom view

Fig. 21 A parametric lofted half wing with a rounded tip

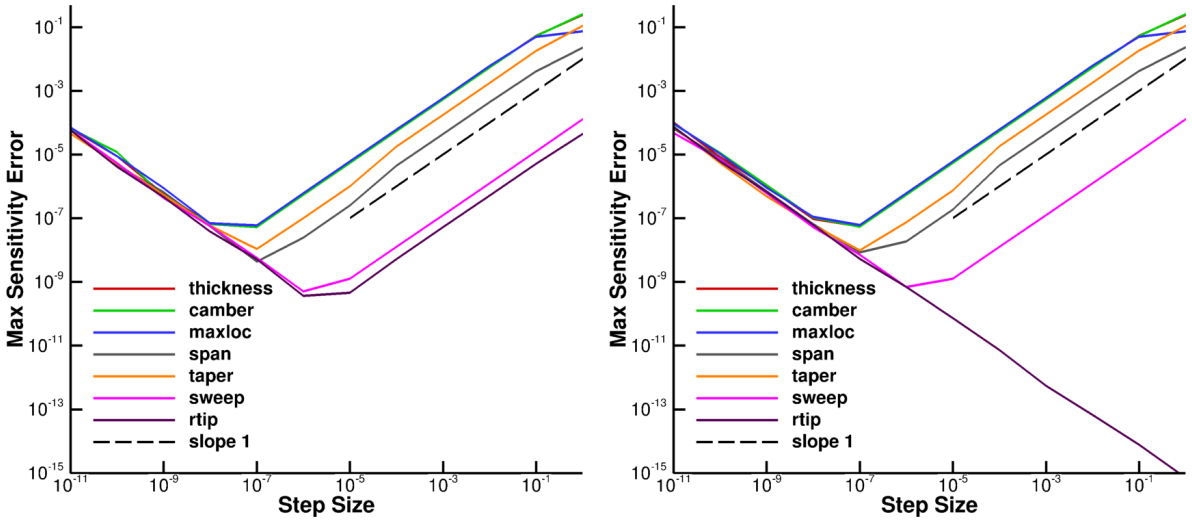

(a) Blunt trailing edge

(b) Sharp trailing edge

Fig. 22 Convergence between 1^{st}-order finite difference and analytic sensitivities

Contours of the inner product between surface normals and parametric sensitivities w.r.t. *camber*, *maxloc*, and *thickness* are shown in Fig. 23. Contours in red represent an outward sensitivity direction from the *solid*, and blue contours show an inward sensitivity direction. As expected, the *camber* parameter has an outward velocity on upper surface, and an inward velocity on the lower surface. For the *maxloc* parameter the fore portion of the upper surface has an inward velocity while the aft portion has an outward velocity. The sign of the velocity is reversed on the lower surface. For both *camber* and *maxloc*, the contours smoothly extend to the rounded tip. The *thickness* parameter has an outward velocity on all surface. However, the maximum velocity actually occurs on the tip of the rounded surface as the $\left\|\vec{b}\right\|$ is proportional to the thickness of the airfoils.

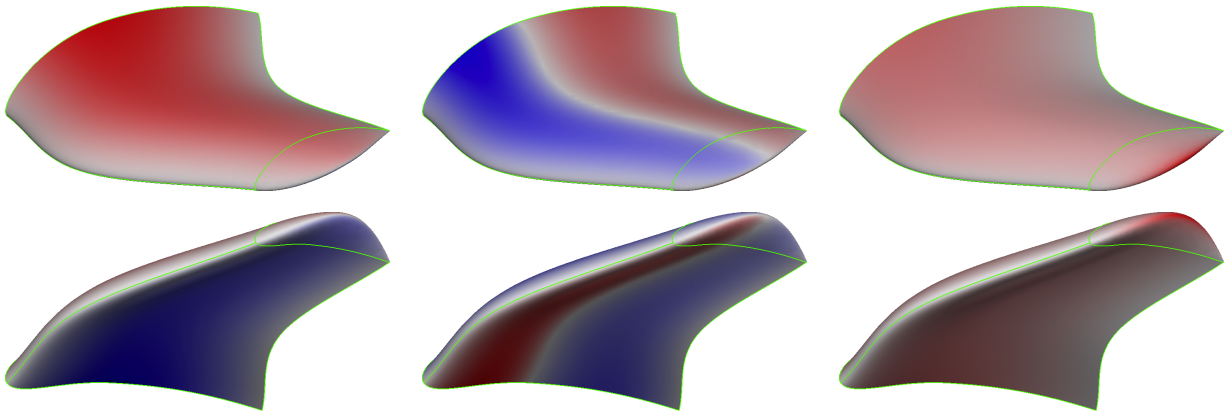

(a) camber

(b) maxloc

(c) thickness

Fig. 23 Configuration parametric sensitivity contours relative to surface normals

V. Conclusion

A $G1$-continuous general elliptic formulation for generating rounded wingtips is presented. The formulation only has a single design parameter intended for preliminary design and is implemented within the ESP geometry generation software. The relatively simple formulation can generate relatively complex rounded wing tips that continue sweep, taper, and twist through the rounded surface. Blunt trailing edges are accounted for by lofting the trailing edge surface into the rounded tip surface. Finally, the correctness of the analytic differentiation of all the spline fitting routines is verified via a finite difference analysis.

Appendix

A few extreme rounded tip shapes are show here.

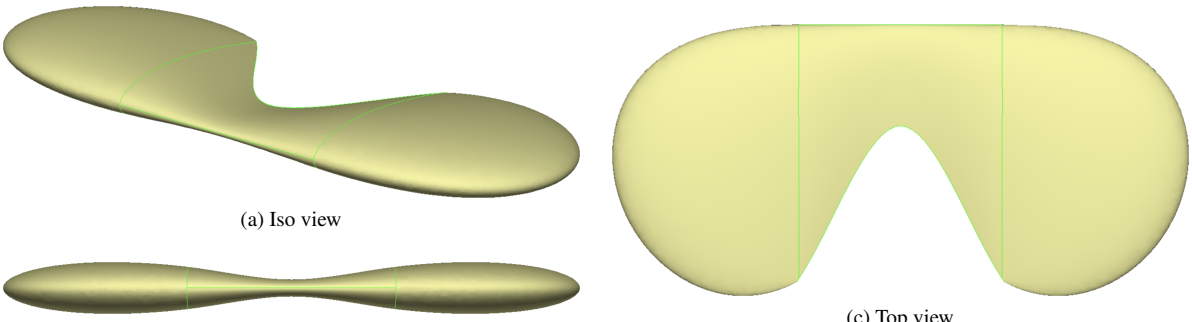

(a) Iso view

(b) Front view

(c) Top view

Fig. 24 Pilot wing with $r = 10$ rounded tip

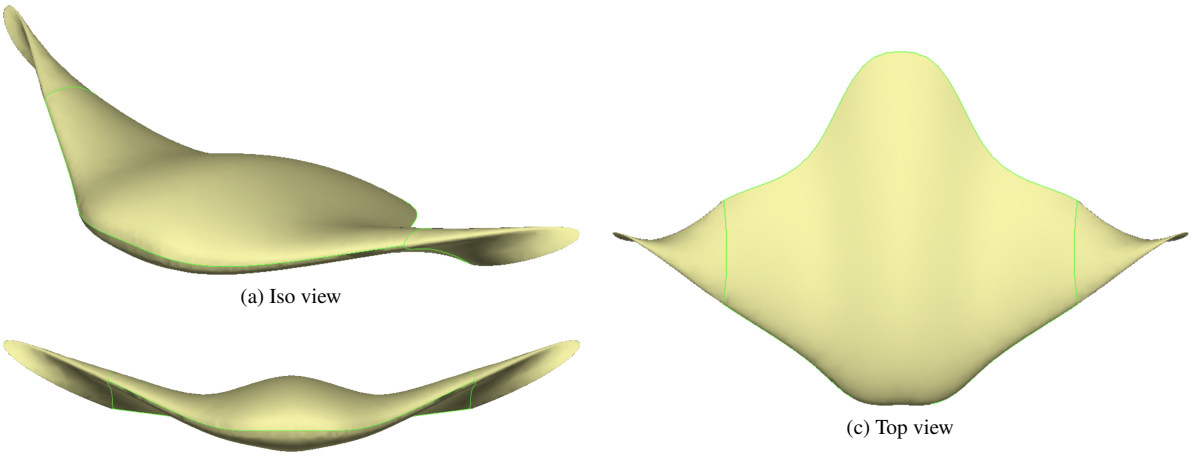

(a) Iso view

(b) Front view

(c) Top view

Fig. 25 Manta ray with $r = 15$ rounded tip

Acknowledgments

The authors would like to tank Prof. John F. Dannenhoffer, III for his efforts developing OpenCSM and for providing example wings with rounded tips. This work was funded by the EnCAPS project, AFRL Contract FA8650–20–2–2002: "EnCAPS: Enhanced Computational Aircraft Prototype Syntheses", with Dr. Ryan Durscher is the Technical Monitor.

References

[1] Alyanak, E., Durscher, R., Haimes, R., John F. Dannenhoffer, I., Bhagat, N., and Allison, D., "Multi-fidelity Geometry-centric Multi-disciplinary Analysis for Design," AIAA 2016-4007, June 2016.

[2] Bryson, D. E., and Haimes, R., "Toward the Realization of a Highly Integrated, Multidisciplinary, Multifidelity Design Environment," AIAA 2019-2225, January 2019.

[3] Haimes, R., and Dannenhoffer, J., "The Engineering Sketch Pad: A Solid-Modeling, Feature-Based, Web-Enabled System for Building Parametric Geometry," AIAA 2013–3073, 2013.

[4] Dannenhoffer, J. F., "OpenCSM: An Open-Source Constructive Solid Modeler for MDAO," AIAA 2013-0701, January 2013.

[5] Chan, W. M., Pandya, S. A., Rogers, S. E., Jensen, J. C., Lee, H. C., Kao, D. L., Buning, P. G., Meakin, R. L., Boger, D. A., and Nash, S. M., *Chimera Grid Tools User's Manual: Version 2.2*, NASA Ames Research Center, Moffett Field, Calif, June 2018. URL `https://www.nas.nasa.gov/publications/software/docs/chimera/index.html`.

[6] Hahn, A. S., "Vehicle Sketch Pad: A Parametric Geometry Modeler for Conceptual Aircraft Design," AIAA 2010-0657, 2010.

[7] Rodriguez, D. L., and Sturdza, P., "A Rapid Geometry Engine for Preliminary Aircraft Design," AIAA 2006-929, January 2006.

[8] Bowcutt, K. G., "A Perspective On The Future Of Aerospace Vehicle Design," AIAA 2003-6957, 2003.

[9] Gagnon, H., and Zingg, D. W., "Geometry Generation of Complex Unconventional Aircraft with Application to High-Fidelity Aerodynamic Shape Optimization," AIAA 2013-2850, January 2013.

[10] Hwang, J., and Martins, J. R. R. A., "GeoMACH: Geometry-Centric MDAO of Aircraft Configurations with High Fidelity," AIAA 2012–5605, September 2012.

[11] Cohen, E., Haimes, R., and Riesenfeld, R., "A Curvature Smooth Lofting Scheme for Singular Point Treatments," *In: Boissonnat JD. et al. (eds) Curves and Surfaces*, Lecture Notes in Computer Science, Vol. 9213, Springer, Cham, 2014, pp. 129–150.

[12] Haimes, R., and Drela, M., "On The Construction of Aircraft Conceptual Geometry for High-Fidelity Analysis and Design," AIAA 2012–683, 2012.

[13] Galbraith, M. C., Allmaras, S. R., and Darmofal, D. L., "A verification driven process for rapid development of CFD software," AIAA 2015-0818, January 2015. https://doi.org/10.2514/6.2015-0818.

[14] Dannenhoffer, J., and Haimes, R., "Design Sensitivity Calculations Directly on CAD-based Geometry," AIAA 2015-1370, 2015.